Journal of Colloid and Interface Science 646 (2023) 576–586

Contents lists available at ScienceDirect

Journal of Colloid And Interface Science

journal homepage: www.elsevier.com/locate/jcis

Multimodal silver-chitosan-acylase nanoparticles inhibit bacterial growth and biofilm formation by Gram-negative *Pseudomonas aeruginosa* bacterium

Guillem Ferreres [a], Kristina Ivanova [a], Juan Torrent-Burgués [a], Tzanko Tzanov [a,*]

[a] *Grup de Biotecnologia Molecular i Industrial, Department of Chemical Engineering, Universitat Politècnica de Catalunya, Rambla Sant Nebridi 22, Terrassa 08222, Spain*

GRAPHICAL ABSTRACT

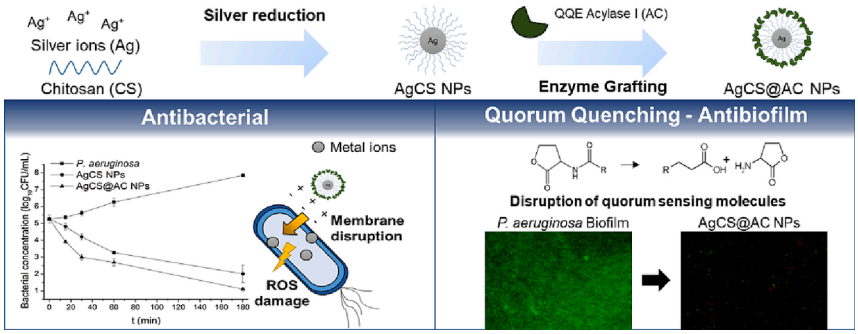

ARTICLE INFO

Keywords:
Silver-chitosan nanoparticles
Acylase
Antimicrobial activity
Quorum quenching
Biofilm inhibition

ABSTRACT

Pseudomonas aeruginosa bacteria originate severe infections in hospitalized patients and those with chronic debilitating diseases leading to increased morbidity and mortality, longer hospitalization and huge financial burden to the healthcare system. The clinical relevance of *P. aeruginosa* infections is increased by the capability of this bacterium to grow in biofilms and develop multidrug resistant mechanisms that preclude conventional antibiotic treatments. Herein, we engineered novel multimodal nanocomposites that integrate in the same entity antimicrobial silver nanoparticles (NPs), the intrinsically antimicrobial, but biocompatible biopolymer chitosan, and the anti-infective quorum quenching enzyme acylase I. Acylase present in the NPs specifically degraded the signal molecules governing bacterial cell-to-cell communication and inhibited by ~ 55 % *P. aeruginosa* biofilm formation, while the silver/chitosan template altered the integrity of bacterial membrane, leading to complete eradication of planktonic bacteria. The innovative combination of multiple bacteria targeting modalities resulted in 100-fold synergistic enhancement of the antimicrobial efficacy of the nanocomposite at lower and non-hazardous towards human skin cells concentrations, compared to the silver/chitosan NPs alone.

* Corresponding author.
E-mail address: tzanko.tzanov@upc.edu (T. Tzanov).

https://doi.org/10.1016/j.jcis.2023.04.184
Received 1 February 2023; Received in revised form 19 April 2023; Accepted 30 April 2023
Available online 5 May 2023
0021-9797/© 2023 The Authors. Published by Elsevier Inc. This is an open access article under the CC BY-NC license (http://creativecommons.org/licenses/by-nc/4.0/).

1. Introduction

Gram-negative pathogenic bacterium *Pseudomonas aeruginosa* is the leading cause of 20 % of the severe healthcare-associated infections, including endophthalmitis, meningitis and pneumonia [1–3]. The appearance of antimicrobial resistance via mutations propelled by natural selection and the ability of this bacterium to switch from a free-floating to a drug resistant biofilm mode of growth under the control of quorum sensing (QS), further increase the significance and negative impact of *P. aeruginosa* associated infections on public health and healthcare [4,5]. QS is a mechanism that allows bacteria to communicate through specific signals excreted in the extracellular environment [6] enabling the single cells to sense the number of bacteria in their environment, and turn on virulence factors expression and biofilm formation [7].

Bacterial biofilms are structures of coordinated surface-adherent communities of bacterial cells, which are enclosed in a self-produced extracellular matrix composed mainly of exopolysaccharides (EPS), proteins and nucleic acids [8]. Biofilm-growing bacteria overwhelm the host immune system response and are up to 1000 times more resistant to conventional biocides and antibiotics when compared to planktonic microorganisms [9]. Different strategies to reduce the incidence of difficult to treat *P. aeruginosa* biofilm infections and improve the clinical outcomes of conventional antibiotic treatments have been proposed. Of note are the anti-QS approaches based on enzymes degrading the signals in the extracellular space or chemical compounds blocking the recognition of the QS signals [10–13]. Recently, the combination of anti-QS actives, such as enzymes, phenolic compounds and cinnamaldehyde, with metal nanoparticles (NPs) have gained attention to avoid the use of antibiotics and prevent from resistance appearance [14–16]. The unique physical properties such as larger surface area to volume ratio of metal NPs allow better interaction with bacterial cells and enhanced penetration into the target site, resulting in high killing performance even against multi-drug resistant bacterial species [17]. However, these highly bactericidal nano-actives are toxic towards human cells and some of them may also provoke resistance appearance [18]. Our group has combined various metal NPs with bioactive components to enhance the metallic NP biocompatibility and at the same time boost their antibacterial efficacy at lower dosages [19–21].

In this work, we developed novel multimodal nano-hybrids comprised of antimicrobial silver/chitosan NP templates conjugated with quorum quenching enzyme (QQE) acylase that integrate complementary activities in a single nano-entity to achieve superior antibacterial and antibiofilm efficacy. Technologically simple, relatively fast and ecologically acceptable synthesis was employed for the production of the hybrid biopolymer-AgNPs using the intrinsically antimicrobial chitosan as both reducing and capping agent. This approach brings multiple benefits not found in the AgNPs alone, including enhanced colloidal stability, biocompatibility and bactericidal activity due to improved interaction and disruption of bacterial membranes [22]. Chitosan also provides functional groups for further grafting of the anti-infective and antibiofilm enzyme acylase on the NPs. Acylase functionalisation of the antibacterial hybrid chitosan-Ag NPs is envisaged to selectively degrade acyl homoserine lactone (AHL) messengers involved in the intercellular communication of *P. aeruginosa*, thereby attenuating its virulence, impeding the formation of biofilm, and increasing the pathogeńs susceptibility to lower dosages of the antimicrobial agent [11,23,24]. The incorporation of multiple bacteria targeting modalities in one nanostructure is expected to synergistically enhance their antibacterial and antibiofilm activities at non-toxic to mammalian cells concentrations. Furthermore, the membrane-disturbing capacity due to the nano-form could reduce the possibility of resistance development and potentiate the major pathways of the antimicrobials for inhibition or eradication of pathogens, such as cell wall synthesis, protein synthesis, nucleic acid synthesis, and metabolic process. The combination of several mechanisms of antibacterial action in a single nano-entity makes these nano-composites of great promise for overcoming the antimicrobial resistance [25–28]. The synergy of the nano-formulated inorganic/bio-based hybrid NPs was validated *in vitro* using planktonic and sessile *P. aeruginosa* cells, and reporter *C. violaceum* biosensor for quorum quenching detection. In order to elucidate the mechanisms of antimicrobial action of the NPs, we studied their interaction with mimetic Gram-negative bacterial membrane using Langmuir isotherms. Finally, *in vitro* tests were performed to assess the cytotoxicity of the novel NPs on human fibroblast cells.

2. Materials and methods

2.1. Reagents and enzymes

50 kDa chitosan (degree of deacetylation – 86.7 %) was obtained from Kitozyme. Silver nitrate, acylase I (E.C 3.5.1.14, 4.5 % (w/w) protein content and 2.49 U mg^{-1} specific activity, pI = 2.3) from *Aspergillus mellus*, crystal violet, acetic acid, Muller-Hinton Broth (MHB), Cetrimide agar, *N*-acetyl-L-methionine, cobalt chloride, ninhydrin reagent, *N*-hexanoyl-DL-homoserine lactone and Dulbecco's Modified Eagle's Medium – high glucose (DMEM) were purchased from Sigma-Aldrich (Spain). 1-Ethyl-3-(3-dimethylaminopropyl)carbodiimide (EDC), *N*-hydroxysulfosuccinimide (NHS), AlamarBlue cell viability reagent, LIVE/DEAD™ viability/cytotoxicity kit for mammalian cells and LIVE/DEAD™ BacLight™ viability kit for bacterial cells were obtained from Thermo Fischer Scientific (Spain). *Pseudomonas aeruginosa* (ATCC 10 145), human fibroblast (ATCC-CRL-4001, BJ-5ta) and keratinocyte (HaCaT) cells were obtained from the American Type Culture Collection (ATCC LGC Standards, Spain). *Chromobacterium violaceum* CECT 5999 (*C. violaceum* CV026), a mini-Tn5 mutant of the wild-type *C. violaceum*, was provided from Spanish Type Culture Collection (CECT, Spain). The lipids phosphatidylethanolamine (PE) and phosphatidylglycerol (PG), extracted from *Escherichia coli*, were obtained from Avanti Polar Lipids, Inc. (Alabama, USA). The precise composition of the myriad corresponding to each headgroup can be found at https://www.avantilipids.com PE (♯ 840027), and PG (♯ 841188). All other chemical and microbiological reagents were purchased from Sigma-Aldrich unless otherwise specified.

2.2. Hybrid AgCS@AC nanoparticles synthesis

Chitosan capped silver (AgCS) NPs were synthesized according to a previously described procedure [29]. Briefly, 1 % (w/v) chitosan solution with pH 5.5 was prepared in 1 % (v/v) acetic acid. Then, 30 mL of 1 % (w/v) chitosan solution were mixed with 20 mL of 2 mg mL^{-1} silver nitrate solution and the mixture was stirred for 3 days at 75 °C in a dark. The obtained NPs were incubated with 4 mg mL^{-1} of acylase at pH 5.5 for 30 min under vigorous stirring. After that, 50 mM of EDC 1-ethyl-3-(3-dimethylaminopropyl)carbodiimide hydrochloride) and 20 mM of *N*-hydroxysulfosuccinimide were added and the mixture was incubated for 2 h at room temperature. The obtained acylase functionalized NPs (AgCS@AC) were washed twice with miliQ water by centrifugation at 18 000 g for 30 min and resuspended in miliQ water for further analysis.

2.3. Nanoparticles characterization

Nanoparticles tracking analysis (NTA, NanoSight NS 300 - Malvern Instruments Inc., UK) in flow mode and software NTA 3.2 were used to capture several frames of the NPs suspension to obtain the hydrodynamic size and final concentration of the particles. ζ- potential of the NPs was measured using a Zetasizer Nano ZS (Malvern Instruments Inc., UK). The reported average values represent the mean values ± standard deviations of five measurements per sample. JEOL JEM-2100 LaB6 transmission electron microscope (TEM) operating at an accelerating voltage of 200 kV was used to assess the size and morphology of the NPs. The sample was prepared by dropping the NPs solution on SiO_2 grids. Energy

dispersive X-ray spectroscopy (EDX) chemical maps were acquired in scanning TEM (STEM) mode using a high angle annular dark field (HAADF) detector to reveal the chemical composition of the NPs. The used spectrometer is an Oxford Instruments INCA x-sight with Si (Li) detector and the maps were acquired using the INCA Microanalysis Suite version 4.09 software.

The amount of silver in AgCS and AgCS@AC NPs was assessed using inductively coupled plasma mass spectrometry (ICP-MS) technique. The samples preparation consisted in mixing 50 μL of the NPs suspensions with 500 μL of 20 % nitric acid. Then, the samples were incubated for 60 min at 100 °C to dissolve completely the silver. After that, the volume was completed to 5 mL with ultrapure water to achieve a final concentration of 2 % of nitric acid. The samples were filtered to remove any solid remaining and measured using ICP-MS 7800, Agilent Technologies calibrated by internal standard with ^{45}Rh and a standard curve of ^{107}Ag.

Acylase activity of the AgCS@AC NPs was tested by mixing the NPs suspension with $CoCl_2$ in tricine buffer. The mixture was incubated at 37 °C, after that 20 mM of *N*-acetyl-L-methionine was added to the solution. The reaction was carried out at 37 °C for 30 min. Then, the mixture was incubated at 100 °C for 3 min to stop the reaction, and cooled at room temperature. 400 μL of 2 % (w/v) ninhydrin reagent solution and 40 μL of 1.6 % (w/v) tin chloride solution were added to the mixture and the reaction was kept for 20 min at 100 °C. The observed colour change was measured at λ = 540 nm in a microplate reader Infinite M200, Tecan (Austria). The same procedure, without the substrate, was performed in order to eliminate the influence of chitosan and proteins present in the particles in the ninhydrin reaction. The specific activity of acylase functionalized NPs was expressed in percentage of the remaining catalytic activity compared to the activity of the enzyme in its free form. The NPs were analysed spectrophotometrically over the 230–930 nm range, using the microplate reader Infinite M200. In addition, lyophilised chitosan, AgCS NPs and AgCS@AC NPs were subjected to FTIR analysis performing 64 scans over 4000–650 cm^{-1} wave number range with PerkinElmer Spectrum 100 (PerkinElmer, Massachusetts, USA). The base line was corrected and the spectra were normalised by the absorbance intensity of the signal in the region at ~ 1030 cm^{-1} with the software PerkinElmer Spectrum.

2.4. Antibacterial activity of AgCS@AC NPs

The antibacterial activity of AgCS@AC NPs was assessed towards *Pseudomonas aeruginosa*. Bacteria were grown overnight at 37 °C in Mueller Hinton broth (MHB). Then, 50 μL of the NPs solutions (silver content from 2 to 50 ppm) were mixed with 50 μL of the bacterial inoculum at optical density (OD) at λ = 600 nm (OD_{600}) = 0.01 (~10^5 –10^6 colony forming units (CFU)·mL^{-1}) in 96-well polystyrene plates. The samples were incubated for 24 h at 37 °C with shaking at 230 rpm. The bacterial growth in presence of the AgCS and AgCS@AC NPs was measured (OD_{600}) in a microplate reader. Samples without turbidity (OD_{600} ~ 0) were considered antibacterial. In addition, the number of survived bacteria during the NPs treatment was determined after plating 10 μL of the suspensions onto cetrimide agar followed by incubation for 24 h at 37 °C and subsequent plate counting on the colonies. All results are reported as mean values ± standard deviations (n = 3).

2.5. Time-kill curves of AgCS@AC NPs

For the time-killing assay, AgCS and AgCS@AC NPs were mixed with *P. aeruginosa* inoculum in MHB at OD_{600} = 0.01 (~10^5 –10^6 CFU·mL^{-1}). At defined time points the samples were diluted and plated in cetrimide agar to count the survived bacterial cells. All results are reported as mean values ± standard deviations (n = 3).

2.6. Langmuir experiments

The interaction of the NPs with biological membranes was studied using Langmuir isotherm. Mixture of phosphatidylethanolamine (PE): phosphatidylglycerol (PG) in a ratio of 8:2 was used to simulate Gram-negative bacterial membrane, since they represent 90 % of the outer membrane phospholipids. The monolayers were formed in a Langmuir trough (KSV NIMA Langmuir–Blodgett Deposition Troughs, model KN2002, Finland) equipped with two mobile barriers mounted on an antivibration table housed in an insulation box at 23 ± 1 °C. The surface pressure (π) was measured using a Wilhelmy plate connected to the trough. The system was cleaned with chloroform and water. The experiments were performed with a barrier closing rate of 15 cm^2·min^{-1}. 30 μL of the phospholipid mixture at a concentration of 0.5 mg mL^{-1} dissolved in chloroform was gently added on a PBS subphase in absence or presence of NPs. The recording of the surface pressure-area per molecule (π-A) isotherm started after 15 min of lagging for complete chloroform evaporation. All the experiments were carried out at least three times for reproducibility. The physical states of the monolayers were assessed by the inverse of the compressibility modulus C_s^{-1} that is obtained from the π-A isotherms calculated using the following equation [30]:

$$C_s^{-1} = -A\left(\frac{d\pi}{dA}\right)_T$$

Where A is the mean area per molecule (Å^2·molecule^{-1}), π the surface pressure (mN·m^{-1}) and T the absolute temperature (K).

2.7. Quorum quenching assay

A single colony of *C. violaceum* CECT 5999 was incubated in Luria-Bertani (LB) medium at 27 °C and 180 rpm for 16 h. After the incubation, bacteria were mixed with LB soft agar to a final concentration of OD_{600} = 0.01. The media was supplemented with kanamycin (25 μM), and 5 mL of this mixture were poured into previously prepared LB agar plates in order to grow a bacterial lawn. The quorum quenching bioassay was performed preparing a reaction mixture with 100 μL of 5 mM PBS pH 7.4, 10 μM of *N*-acetyl homoserine lactone (AHL), 500 μM of $CoCl_2$ and 100 μL of AgCS@AC NPs, the free acylase or the stand-alone AgCS NPs, at the same protein and silver concentration, respectively. The samples were incubated for 5 h at 37 °C. Then, 10 μL of each reaction were used to soak sterile filter papers of 5.5 mm. The papers were then placed on the previously prepared LB agar and incubated at 27 °C for 16 h. The anti-QS activity of acylase-decorated NPs was confirmed by the decrease of the violet halo in comparison to the control containing only the AHL. Finally, the images were analysed using the software ImageJ in order to assess the intensity of the colour production. The results were express as a percentage of colour intensity regarding the plates with AHLs without QQE acylase.

2.8. Biofilm inhibition by AgCS@AC NPs

The biofilm inhibition activity of the synthesized NPs was assessed towards *Pseudomonas aeruginosa*. *P. aeruginosa* inoculum was prepared in tryptic soy broth (TSB) (OD_{600} = 0.01) and incubated with the NPs for 24 h at 37 °C in a 96 well plate to allow the biofilm formation. 0.1 mg mL^{-1} of free acylase was used as control. The formed biofilm was washed three times with 150 μL of 100 mM phosphate buffered saline, pH 7.2 (PBS) and fixed to the well for 1 h at 55 °C. Subsequently, the attached biofilm was stained by incubation with 0.1 % (w/v) crystal violet for 15 min. Excess of staining solution was removed by three gentle washings with water, and finally 200 μL of 30 % (v/v) acetic acid was added to each well to solubilize the crystal violet bound to the biofilm cells and extracellular matrix. A volume of 130 μL of the solution was transferred to a new plate and the absorbance was measured at λ = 595 nm. The amount of crystal violet staining in the assay is directly proportional to the biomass that is attached to the plate [31]. All results are reported as mean values ± standard deviations (n = 3).

Alternatively, after the biofilm washing step, 20 μL of the LIVE/DEAD BacLight™ Bacterial Viability kit prepared in PBS were added to each well and the images of the live and dead cells within the biofilm were taken with a microscope Nikon/Eclipse Ti − S (The Netherland).

2.9. Cytotoxicity assessment of AgCS@AC NPs

Human fibroblast cell line BJ5tα and human keratinocytes cell line HaCaT were used to determine the toxicity of the hybrid NPs toward mammalian cells as previously described [32]. In a 96 well plate, $6{\cdot}10^4$ cells were placed in each well. NPs suspensions, at their antibacterial effective concentrations, were placed in contact with the previously cultured cells. After 24 h of contact, the particles were removed and fresh media was added to each well. Then, the cells were left for 24 h at 37 °C for complete recovery and the number of viable cells was quantified using AlamarBlue assay kit (AlamarBlue, Invitrogen). All results are reported as mean values ± standard deviations (n = 3). In parallel, 20 μL of a PBS solution containing 0.1 % (v/v) of calcein AM and 0.1 % (v/v) of ethidium homodimer-1 were added to each well and the cells were left for 15 min in the dark. The non-reacted stains were then washed with PBS, and the live and dead cells were observed using a fluorescence microscope (Nikon/Eclipse Ti − S, The Netherlands).

3. Results and discussion

3.1. Synthesis and characterization of hybrid AgCS@AC NPs

At first, monodisperse AgCS NPs with a hydrodynamic diameter of ~ 140 nm and ζ- potential of 51 ± 2.8 mV were produced within 3 days of incubation of silver nitrate with chitosan under stirring at 75 °C (Fig. 1A). UV–vis spectrophotometry further revealed a peak at 420 nm due to the typical surface plasmon resonance signal of AgNPs related to the collective oscillations of their conduction electrons, thereby confirming the synthesis of the metal NPs (Fig. 1B) [33–35]. The FTIR spectrum of the NPs further demonstrated the formation of nano-composite. The mechanism for Ag-chitosan NPs generation starts with the interaction of Ag^+ with the $–NH_2$ and –OH groups of chitosan, confirmed by the changes of the bands between ~ 3500 and 3300 cm^{-1} (–OH and –NH) and at ~ 1550 cm^{-1} (–NH) in the chitosan spectrum [36,37]. Thereafter, the reduction in the –OH signal and the appearance of band at ~ 2850 cm^{-1} (–CH of carboxylic groups), ~1730 (C═O), and ~ 1400 cm^{-1}, corresponding to carbonyl and carboxyl groups, indicates the oxidation of the chitosan hydroxyl groups upon the reduction of Ag^+ to Ag^0 [38–40]. The aggregation of the particles is prevented by stabilizing interactions between the metal and the biopolymer [41] (Fig. 1J).

The obtained AgCS NPs were further functionalized with the QQE acylase I using EDC and NHS cross-linking reaction between the amino groups present in the chitosan shell of the NPs and carboxylic groups from the protein, producing AgCS@AC nano-hybrids [42]. Grafting negatively charged acylase (with a ζ-potential of −11 ± 0.9 mV) onto the AgCS NPs resulted in a decrease of the AgCS NPs surface charge from 51 ± 2.8 mV to 22.6 ± 0.35 mV. When this nano-composite was analysed via UV–vis spectroscopy, the peak at 420 nm related to AgNPs was still present and a new peak at 250 nm, corresponding to the aromatic residues of the enzyme protein was observed (Fig. 1B) [43]. In addition, TEM analysis showed that the spherical AgCS NPs with a size between 25 and 30 nm were embedded in a protein matrix (Fig. 1C, D and F). In addition, the high-angle annular dark field (HAADF) mapping STEM confirmed the presence of both sulphur from cysteine lateral residues of the enzyme (Fig. 1H) and silver (Fig. 1I) in the same nano-entity, indicating the successful synthesis of the hybrid nano-composite. Furthermore, in the FTIR spectrum of AgCS@AC NPs, amide I and II signals at ~ 1650/~1550 cm^{-1} corresponding to the peptide bond of the enzyme and the newly formed bond promoted by EDC [44]. The signal between ~ 3500 and ~ 3300 cm^{-1} increased due to the –OH lateral residues of the amino acids, reaffirming the presence of acylase I in the nano-composite (Fig. 1K).

Furthermore, the particles containing QQE acylase I were able to hydrolyse *N*-acetyl-L-methionine and produced a colour change from pink to dark purple during the ninhydrin assay [45]. After the cross-linking between the chitosan and the acylase I, the enzyme maintained up to ~ 65 % of its residual activity. On the other hand, AgCS NPs without acylase did not show an important colour change that may appear as a result of ninhydrin interaction with the amine groups present in the chitosan. All these results suggest the capacity of acylase decorated AgCS NPs to interfere with the QS and consequently impede *P. aeruginosa* virulence factors secretion and establishment of biofilms.

3.2. Antibacterial activity of AgCS@AC NPs against P. Aeruginosa

The antibacterial activity of the AgCS NPs and AgCS@AC NPs was assessed towards the Gram-negative *P. aeruginosa*. First, the silver content of the particles was normalized for each sample. At a concentration of silver of 13.28 ppm, all the samples eradicated completely the Gram-negative bacteria, while at 3.32 ppm none of them presented bactericidal efficacy. When the silver content was 6.64 ppm, AgCS@AC NPs presented 100-fold higher antimicrobial activity when compared with the bare AgCS NPs (Fig. 2A). The enhanced antimicrobial efficacy of the hybrid metal/bio-based AgCS@AC NPs is due to the synergistic combination between the antibacterial AgCS NPs template and anti-QS enzyme acylase. AgNPs can produce reactive oxygen species (ROS) damaging the cell membrane, in addition, the released metallic ions can easily penetrate in the bacterial cell, increasing the ROS production and inhibiting important metabolic pathways [46]. Capping AgNPs with cationic biopolymers as chitosan promotes the interaction with the negatively charged bacterial cell surface, producing changes in the membrane permeability that lead to internal cell imbalance and the hydrolysis of the membrane [47]. Furthermore, the addition of acylase in the AgCS NPs shell interrupts the communication between the pathogens and makes them less virulent, cooperatively increasing the bactericidal performance of the nano-formulated silver agent [13,21,48].

In order to confirm the importance of QS attenuation for boosting the killing effect of NPs, we measured bacterial growth inhibition effect of the AgCS NPs at non-bactericidal concentration (3.32 ppm) together with bulk acylase at different amounts (0–50 μg/mL). Previous reports highlighted the importance of the QS in the tolerance of bacteria to antimicrobial agents and oxidative stress [49,50]. Accordingly, our results revealed that quorum quenching acylase increased the susceptibility of *P. aeruginosa* to the AgCS NPs (Fig. 2B).

3.3. Time-killing assay

Time-killing kinetics of the AgCS and AgCS@AC NPs, at 6. 64 ppm silver concentration, were performed to determine the viability of the treated bacteria and define the rate at which the NPs exert their bactericidal properties. The time-killing assay showed a similar tendency as the previous experiment, being the AgCS@AC NPs more effective against *P. aeruginosa* than the AgCS NPs. Both AgCS NPs and AgCS@AC NPs displayed a rapid killing of *P. aeruginosa* and decrease of bacterial live load by 0.6 and 1.4 $\log_{10}$ ($CFU{\cdot}mL^{-1}$), respectively, after 20 min of incubation. Interestingly, when the NPs were combined with QQE acylase I the bacterial reduction and rate of killing were higher (Fig. 3) compared with the control AgCS NPs, confirming the co-adjuvant role of anti-virulent acylase I in enhancing the bactericidal effect of the NPs templates and corroborating the results obtained in the antimicrobial assay (Fig. 2A).

3.4. Interaction of AgCS@AC NPs with a model bacterial membrane

PE and PG are the main phospholipids of the *E. coli* membrane that are used as a model of a Gram-negative bacterial membrane. PE is the

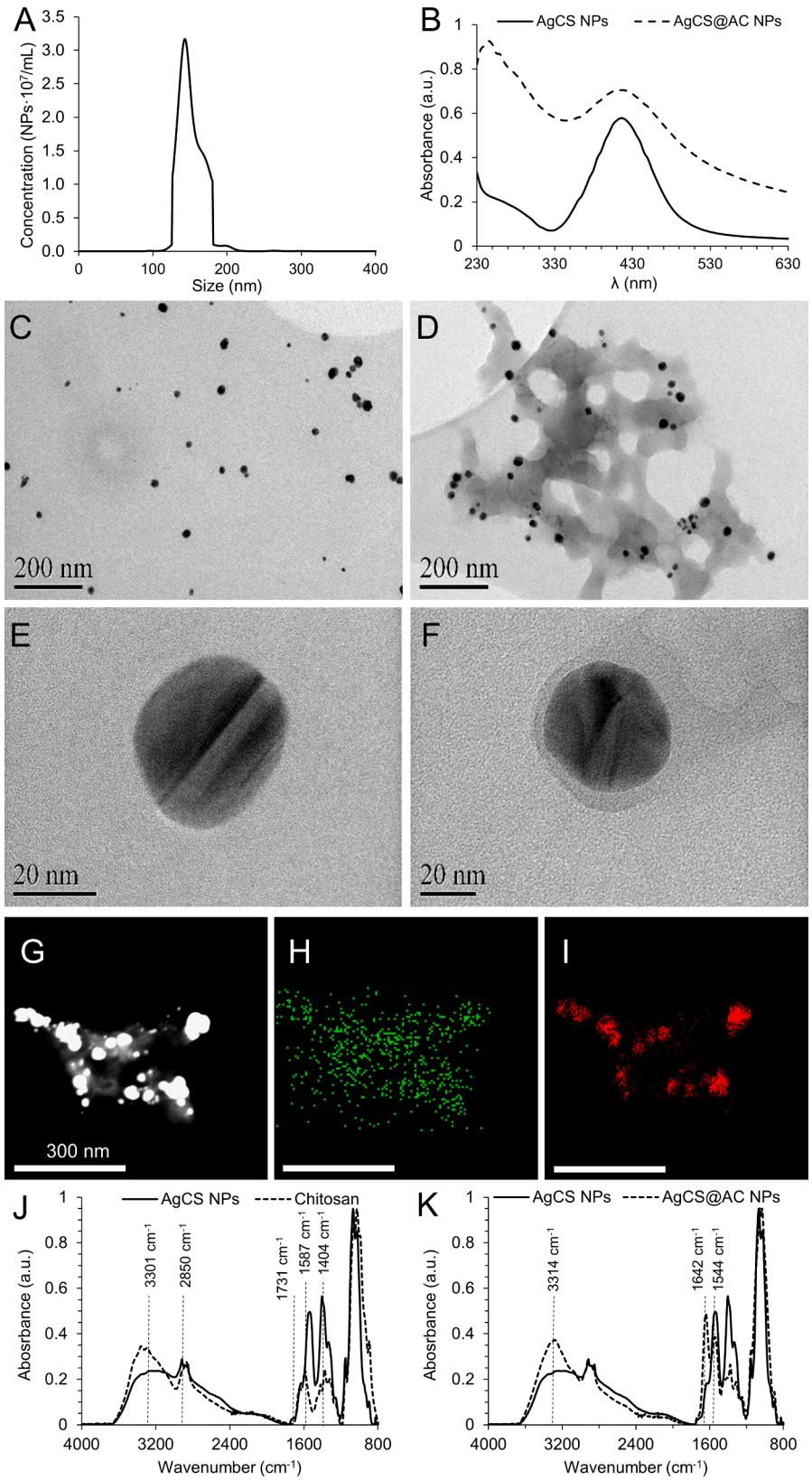

Fig. 1. AgCS NPs and AgCS@AC NPs characterization. A) Size distribution of the AgCS NPs. B) UV–vis spectroscopy of AgCS NPs and AgCS@AC NPs. TEM images of AgCS NPs (C, E) and AgCS@AC NPs (D, E) using the HAADF detector and EDX analysis of the AgCS@AC NPs (G) with elemental analysis of sulphur (H) and silver (I). FTIR spectra of chitosan vs AgCS NPs (J) and AgCS NPs vs AgCS@AC NPs (K).

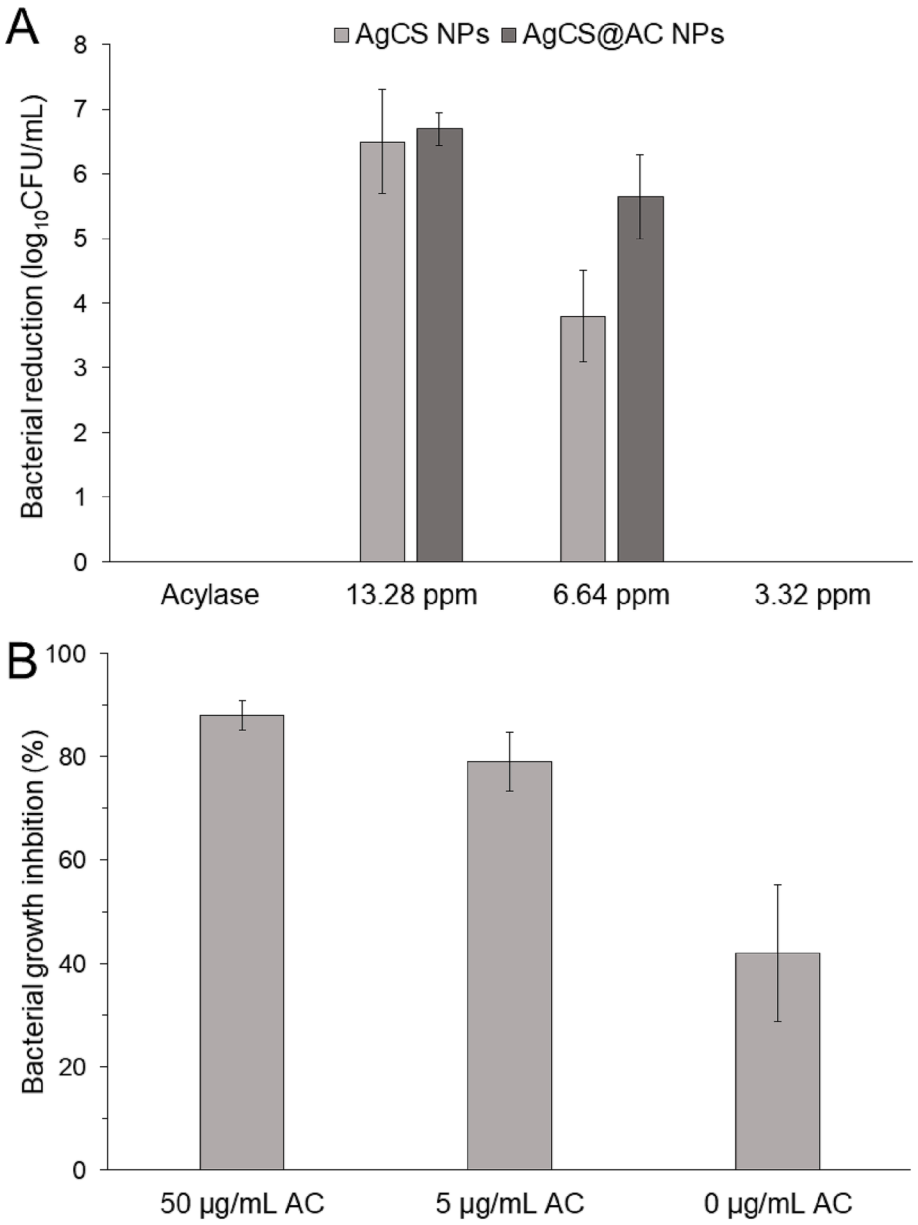

Fig. 2. (A) Evaluation of the antimicrobial activity of AgCS NPs and AgCS@AC NPs. The particles were tested after silver content normalization. The antibacterial activity of Acylase I was tested at the initial concentration employed for the synthesis of the particles. (B) Growth inhibition of *P. aeruginosa* by AgCS NPs, at their non-bactericidal concentration (3.32 ppm silver content), in presence of different concentrations of bulk acylase I.

major component of bacterial membrane and interacts with important membrane proteins, while PG is the second main phospholipid. Both of them represents around 90 % of the total lipid content in Gram-negative bacterial outer membranes [51,52]. These phospholipids were used to record the surface pressure-area isotherm of the monolayer with and without the chitosan containing NPs. As observed in previous works, PE:PG π-A isotherm monotonically increases until its collapse pressure at $\pi = 49$ mN·m^{-1} [53]. The addition of chitosan-containing NPs shifted the initial stage of the isotherm towards higher values of area per molecule, and this effect is maintained throughout the entire isotherm [54]. At a pressure of 33 mN·m^{-1}, physiological pressure of biological membranes, the negatively charges PE:PG monolayer presents an area of ~ 63 Å^2/molecule, the AgCS@AC NPs increased this value to 69 Å^2/molecule while the AgCS NPs reached 85 Å^2/molecule (Fig. 4A). The increase of the area in Langmuir π-A isotherm could be related with the intercalation of the NPs in the phospholipid monolayer, or due the electrostatic interactions between the NPs and the negatively charges phospholipid heads of PG [55]. The higher positive ζ- potential of the AgCS NPs than the AgCS@AC NPs allows better interaction with PG, producing more pronounced displacement of the isotherm to higher values of area. In addition, both NPs decrease the collapse pressure of the monolayer, which may correlate with a reduction of the membrane stability. Herein, we hypothesize that the NPs simultaneously induce destabilization due to insertion into the lipids, and then, stabilization of the negative charges of the monolayer, thus the more positive ζ- potential of the AgCS NPs conferred greater stability to the monolayer than the AgCS@AC NPs. For this reason, the NPs containing enzyme produce the collapse of the mimetic membrane at lower pressure compared to their counterpart without enzyme. It has been previously observed, that chitosan in bulk form at higher pH, when its positive charge is lower, reduced the collapse pressure of negatively charged membranes in comparison with lower pH where the polyion adopts a positive charge [56]. In order to discard the influence of the surface activity of the NPs, the isotherms of the NPs in absences of the phospholipid were assessed and they showed

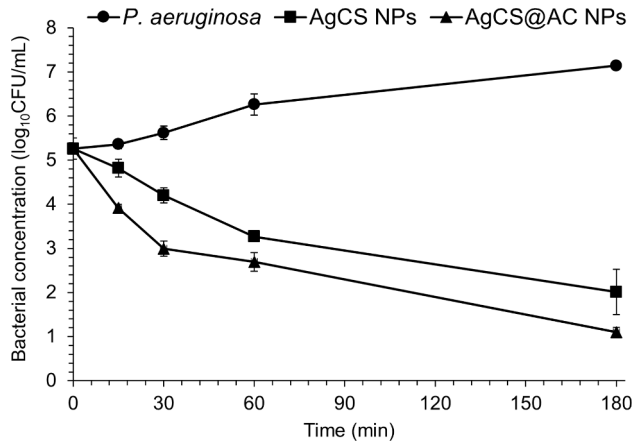

Fig. 3. Time-kill curves of AgCS NPs (square) and AgCS@AC NPs (triangle) towards *Pseudomonas aeru*ginosa (circle). *P. aeru*ginosa was incubated with 6.64 ppm of silver and the bacteria surviving the treatment were estimated after 15, 30, 60 and 180 min.

that the nanostructures do not present effect at areas greater than the collapse points (Fig. 4B). Finally, in the case of the inverse of the compressibility module curves, the PE:PG monolayer is maintained a fluid or liquid state at biological conditions, however AgCS and AgCS@AC NPs decreased the Cs^{-1} values, also at 33 $mN{\cdot}m^{-1}$ (Fig. 4A, inset), indicating a membrane fluidization effect (Fig. 4A) [57].

3.5. Quorum quenching and biofilm inhibition by AgCS@AC NPs

Gram-negative bacteria secrete acyl homoserine lactones and use them as cell-to-cell communication molecules in the QS process. *P. aeruginosa* employs acyl homoserine lactones (AHL), e.g. N-(3-oxo-dodecanoyl)-l-homoserine lactone and *N*-butyryl-l-homoserine lactone, signalling molecules to express a multitude of virulence factors, which enable the bacterium to establish infection, and also form biofilm on various surfaces [58]. Affecting the QS related processes via enzymatic hydrolysis of these signals with acylase I is innovative approach to attenuate bacterial virulence and reduce biofilm-associated infections, increasing the pathogens susceptibility to conventional antimicrobials at lower amounts [59]. Strategies targeting the bacterial molecular mechanisms are reported to exert less evolutionary pressure on the bacterial population and do not provoke development of resistance.

The anti-QS activity of bulk acylase and acylase containing NPs was confirmed through the decrease in the QS-governed violacein production with *C. violacium* CV026. *C. violacium* CV026 is a quorum biosensor strain, derived from *C. violaceum* ATCC 31532, which is not able to produce AHL molecules, therefore in order to synthetize detectable by naked eye purple pigment violacein, the QS signals have to be supplemented externally [60]. The AHL molecules were incubated with the enzyme or the NPs and subsequently, a fraction of the reaction was used to soak a filter paper that was placed on the bacterial lawn. After 16 h, all the plates presented violet halo. The samples that did not contained the QQE displayed a high pigment production, indicating that the QS process remained unaltered (Fig. 5A and 5C). On the other hand, acylase I and AgCS@AC NPs were able to degrade the AHLs and the production of violacein was considerably reduced (Fig. 5B and 5D). The plates presented 30 % lower colour intensity regarding the ones with untreated AHL (Fig. 5E), confirming the quorum quenching activity of the NPs.

The role of QQE acylase in inhibition of biofilm establishment was further assessed. For the biofilm inhibition test, *P. aeruginosa* was exposed to AgCS NPs and AgCS@AC NPs at a concentration that does not present bactericidal activity and incubated in static conditions to allow the establishment of biofilm. The biofilm formation was assessed by crystal violet assay and live-dead staining.

Crystal violet assay is used to indirectly quantify the total biomass formation on the surface by measuring crystal violet-stained carbohydrates in the biofilm extracellular matrix and the cells.[61] At subinhibitory concentration (3.32 ppm), AgCS@AC NPs inhibited the biofilm growth on model polystyrene surface by more than 55 %, while the AgCS NPs at the same concentrations had negligible effect, reducing the *P. aeruginosa* biofilm formation only by 5 % (Fig. 5F). The fluorescence microscopy images corresponding to the live (green)/dead (red) staining assay showed further how the treatment with AgCS NPs reduces the live bacteria in the biofilm, as lower fluorescence intensity and higher number of red zones were observed regarding the control without treatment (Fig. 5G and 5H). Importantly, the treatment with AgCS@AC NPs showed the lowest fluorescence intensity due to the complementary mode of action between the acylase I, inhibiting the QS regulated production of biofilm matrix, and AgCS NPs template that kill the less virulent cells approaching the surface (Fig. 5I).

3.6. Assessment of the potential cytotoxicity of AgCS@AC NPs

Despite that silver has been approved for antimicrobial applications by the US Food and Drug Administration (FDA), silver in its nano-form has been reported to be toxic to human cells [62,63]. Therefore, the toxicity of the developed NPs was tested on two human skin cell lines, namely fibroblast (BJ5tα) and keratinocytes (HaCat) using alamarBlue assay for quantification of the metabolically active cells, and a live/dead viability/cytotoxicity assay kit for microscopic visualization of live and dead cells. The alamarBlue assay consists in the reduction of the alamarBlue® reagent by the metabolic activity of the mammal cells [64]. AgNPs hybridization with natural polymers (e.g. aminocellulose,

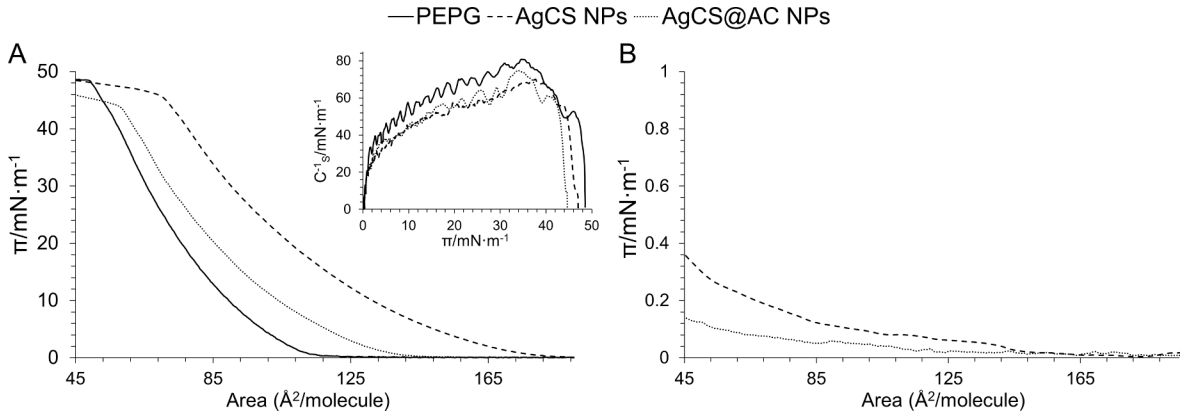

Fig. 4. π-A isotherm of (A) a PE:PG 8:2 monolayer in PBS (solid), with AgCS NPs (dash) and AgCS@AC NPs (dots). Inset: the inverse of the compressibility modulus of the isotherms. (B) π-A isotherm of AgCS NPs (dash) and AgCS@AC NPs (dots) in absence of the phospholipid mixture.

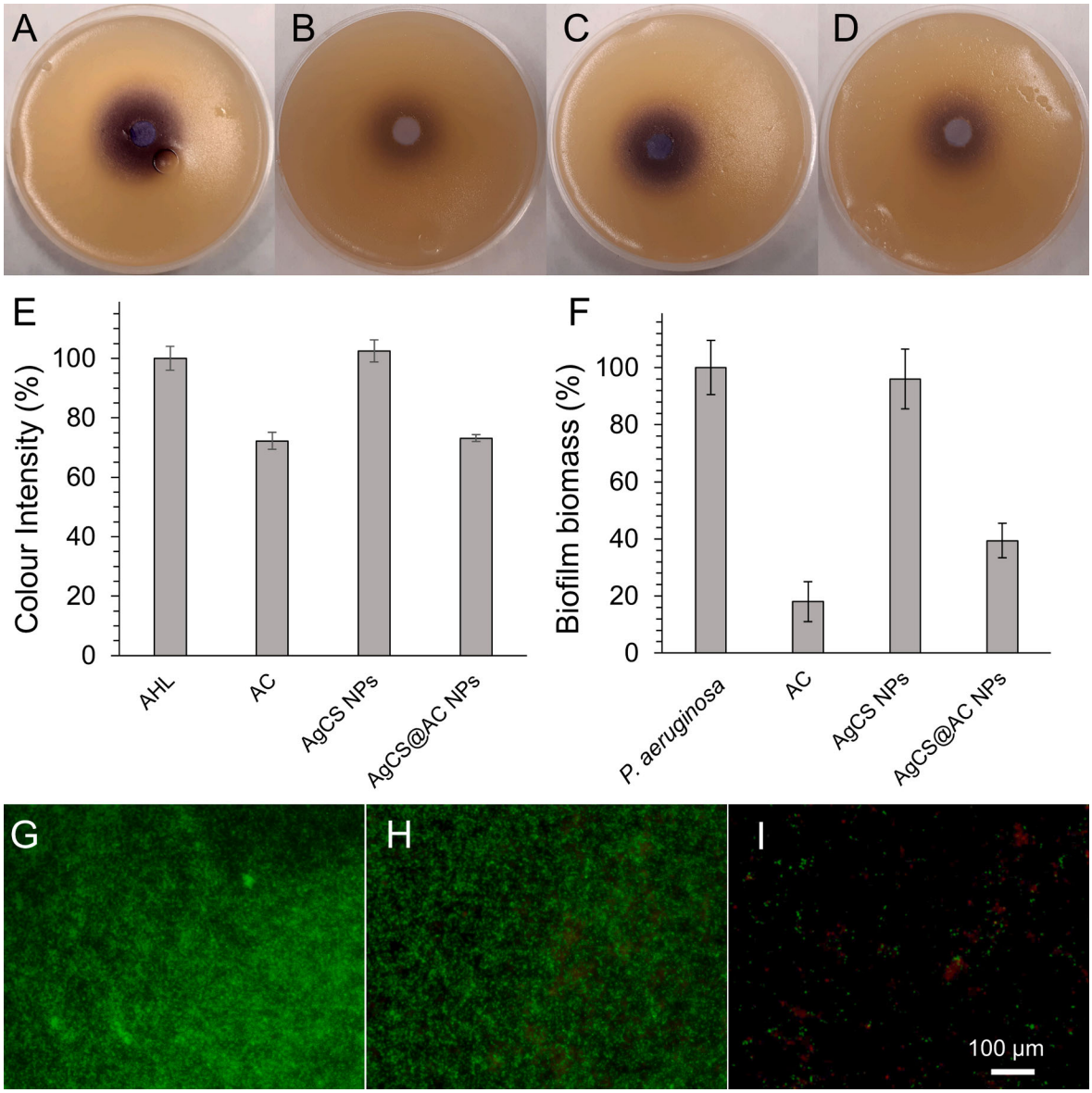

Fig. 5. Quorum quenching assay. *C. violacium* CV026 culturing in a plate with paper disks soaked in AHL solutions (A) with free acylase I (B), AgCS NPs (C), and AgCS@AC NPs (D). Assessment of the changes in the intensity of the colour after 16 h of incubation (E). Evaluation of the biofilm inhibiting activity of AgCS NPs and AgCS@AC NPs. *P. aeruginosa* biofilm inhibition by AgCS NPs and AgCS@AC NPs determined using crystal violet assay (F). Fluorescence microscopy images of *P. aeruginosa* (G) after the treatment with AgCS NPs (H) and AgCS@AC NPs (I). The green and red fluorescence images are overlaid for better comparison. (For interpretation of the references to colour in this figure legend, the reader is referred to the web version of this article.)

chitosan and lignin), has been previously described for reducing the toxicity of nano-silver to human cells [21,65,66]. Further modification of the NPs with acylase I, increased the biocompatibility of the AgCS NPs by ~ 15–20 %. After 24 h of incubation and 24 h of recovery time, at a silver content of 6.64 ppm, the particles with acylase I showed reduced toxic effect on the cells in comparison to the AgCS NPs. Both cell lines treated with AgCS@AC NPs showed more than 80 % of cell viability, while their viability when exposed to AgCS NPs was around 65 % (Fig. 6A). The microscopy images show that the human skin cells after the treatment with NPs did not display apparent changes in their morphology. However, the ones treated with AgCS NPs presented lower cell density and more dead cells (stained in red) when compared with the Acylase I functionalized NPs (Fig. 6B). These results confirm that the toxicity of silver can be reduced upon its combination with biomolecules as chitosan and acylase I.

4. Conclusions

The appearance of multidrug resistant bacteria and the formation of difficult-to-eradicate biofilms on living and non-living surfaces call for the development of new antimicrobials able to deal with these challenges. In this work, we developed novel nano-hybrids with complementary mode of action using AgCS NPs together with acylase I, to inhibit the bacterial pro-pathological cell-to-cell communication process and at the same time eradicate the targeted pathogen. The antibacterial AgCS NPs were synthesised through silver ions reduction by chitosan, avoiding the use of any toxic reagents, and served as templates for further QQE acylase I covalent immobilization. The obtained nanocomposite was able to reduce more effectively both the planktonic bacterial growth and biofilm formation of *P. aeruginosa* than the AgCS NPs alone, without affecting the viability and morphology of human fibroblast and keratinocytes cells. The enhanced bactericidal effect of the novel nano-actives was a result of acylase-quenching of *P. aeruginosa*

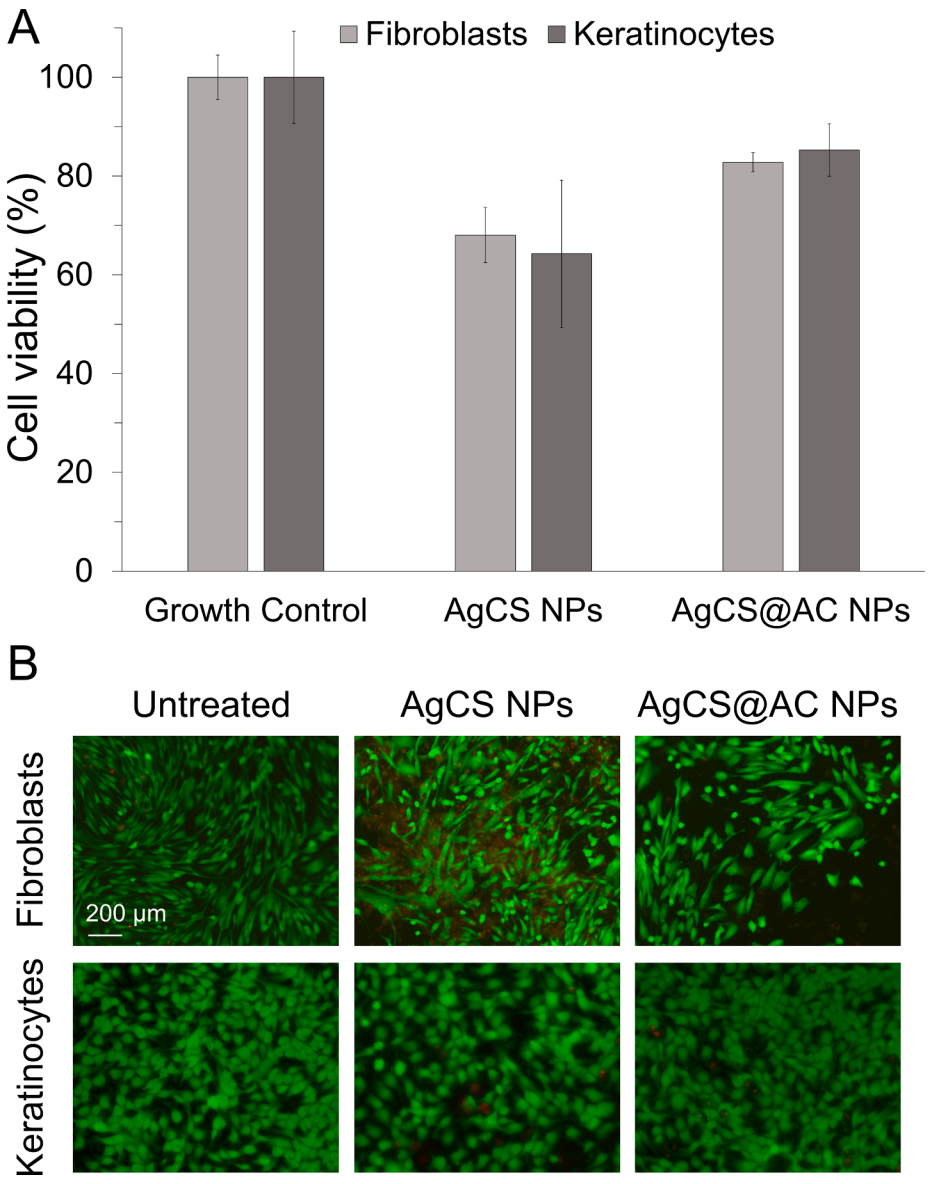

Fig. 6. Cytotoxicity of AgCS NPs and AgCS@AC NPs. A) Alamarblue assay for assessment of the cellular metabolic activity of fibroblast (BJ5tα) and keratinocytes (HaCat) after 24 h of incubation with AgCS NPs and AgCS@AC NPs. B) Fluorescence microscopy images of fibroblast (BJ5tα) and keratinocytes (HaCat) after 24 h of incubation with AgCS NPs and AgCS@AC NPs. The green and red fluorescence images are overlaid for better comparison. (For interpretation of the references to colour in this figure legend, the reader is referred to the web version of this article.)

cell-to-cell communication coupled to improved interaction and destabilization of bacterial membrane by the nano-form. The combination of distinct mechanisms of antibacterial and antibiofilm action in the same nano-entity is an innovative multifactorial approach to attenuate the bacterial virulence, inhibit the biofilm establishment and eradicate the free-floating *P. aeruginosa* cells at lower silver concentration, thus reducing the selective pressure for the appearance of antimicrobial resistance. The developed antibacterial and antibiofilm nano-formulation could be further exploited for coating of medical devices, e.g. urinary catheters and contact lenses, as actives for treatment of skin infections, and in hydrogel dressings to reduce the incidence of biofilm-related infections.

Author contributions

G.F.: NPs synthesis and physical and antimicrobial characterization, Langmuir data acquisition and analysis, manuscript writing. KI.: experiments design, biofilm and quorum quenching experiments, data acquisition, analysis, manuscript writing, figure design. J.T.B.: Langmuir experiments design and analysis, manuscript writing. T.T.: experiments design, manuscript writing and revision, project administration, funding acquisition.

Declaration of Competing Interest

The authors declare that they have no known competing financial interests or personal relationships that could have appeared to influence the work reported in this paper.

Data availability

Data will be made available on request.

Acknowledgment

This work was supported by Spanish Ministry of Economy and Competitiveness Projects (MINECO) CoatToSave—Nanoenabled hydrogel coatings against antimicrobial-resistant catheter-related infections, PID2019-104111RB-I00, and the European project AMROCE - Nano-enabled strategies to reduce the presence of contaminants of emergent concern in aquatic environments, PCI2021-121926. G. F acknowledges Universitat Politècnica de Catalunya and Banco Santander for his PhD

grant (113 FPI-UPC 2018).

References

[1] C.W.G. Eifrig, I.U. Scott, H.W. Flynn, D. Miller, Endophthalmitis caused by Pseudomonas aeruginosa, Ophthalmology. 110 (2003) 1714–1717, https://doi.org/10.1016/S0161-6420(03)00572-4.

[2] A. Frattari, V. Savini, E. Polilli, D. Cibelli, S. Talamazzi, D. Bosco, A. Consorte, P. Fazii, G. Parruti, Ceftolozane-tazobactam and Fosfomycin for rescue treatment of otogenous meningitis caused by XDR Pseudomonas aeruginosa: Case report and review of the literature, IDCases 14 (2018) e00451, https://doi.org/10.1016/j.idcr.2018.e00451.

[3] R.T. Sadikot, T.S. Blackwell, J.W. Christman, A.S. Prince, Pathogen-host interactions in pseudomonas aeruginosa pneumonia, Am. J. Respir. Crit. Care Med. 171 (2005) 1209–1223, https://doi.org/10.1164/rccm.200408-1044SO.

[4] P. Pachori, R. Gothalwal, P. Gandhi, Emergence of antibiotic resistance Pseudomonas aeruginosa in intensive care unit; a critical review, Genes Dis. 6 (2019) 109–119, https://doi.org/10.1016/j.gendis.2019.04.001.

[5] J.W. Costerton, P.S. Stewart, E.P. Greenberg, Bacterial biofilms: A common cause of persistent infections, Science. 284 (1999) 1318–1322, https://doi.org/10.1126/science.284.5418.1318.

[6] K. Brindhadevi, F. Lewisoscar, E. Mylonakis, S. Shanmugam, T. Nath, A. Pugazhendhi, Biofilm and Quorum sensing mediated pathogenicity in Pseudomonas aeruginosa, Process Biochem. 96 (2020) 49–57, https://doi.org/10.1016/j.procbio.2020.06.001.

[7] N. Personnic, B. Striednig, H. Hilbi, Quorum sensing controls persistence, resuscitation, and virulence of Legionella subpopulations in biofilms, ISME J. 1 (2021) 196–210, https://doi.org/10.1038/s41396-020-00774-0.

[8] H.C. Flemming, J. Wingender, The biofilm matrix, Nat. Rev. Microbiol. 8 (2010) 623–633, https://doi.org/10.1038/nrmicro2415.

[9] K. Ivanova, E. Ramon, J. Hoyo, T. Tzanov, Innovative Approaches for Controlling Clinically Relevant Biofilms, Curr. Trends Futur. Prospect. 17 (2017) 1889–1914, https://doi.org/10.2174/1568026617666170105143315.

[10] K. Ivanova, M.M. Fernandes, A. Francesko, E. Mendoza, J. Guezguez, M. Burnet, T. Tzanov, Quorum-Quenching and Matrix-Degrading Enzymes in Multilayer Coatings Synergistically Prevent Bacterial Biofilm Formation on Urinary Catheters, ACS Appl. Mater. Interfaces. 7 (2015) 27066–27077, https://doi.org/10.1021/acsami.5b09489.

[11] K. Ivanova, M.M. Fernandes, E. Mendoza, T. Tzanov, Enzyme multilayer coatings inhibit Pseudomonas aeruginosa biofilm formation on urinary catheters, Appl. Microbiol. Biotechnol. 99 (2015) 4373–4385, https://doi.org/10.1007/s00253-015-6378-7.

[12] Y. Pan, Y. Wang, X. Yan, C. Liu, B. Wu, X. He, Y. Liang, Quorum Quenching Enzyme APTM01, an Acylhomoserine - Lactone Acylase from Marine Bacterium of Pseudoalteromonas tetraodonis Strain MQS005, Curr. Microbiol. 76 (2019) 1387–1397, https://doi.org/10.1007/s00284-019-01739-z.

[13] K. Ivanova, A. Ivanova, J. Hoyo, S. Pérez-Rafael, T. Tzanov, Nano-Formulation Endows Quorum Quenching Enzyme-Antibiotic Hybrids with Improved Antibacterial and Antibiofilm Activities against Pseudomonas aeruginosa, Int. J. Mol. Sci. 23 (2022) 7632, https://doi.org/10.3390/ijms23147632.

[14] G. Vinoj, R. Pati, A. Sonawane, In Vitro Cytotoxic Effects of Gold Nanoparticles Coated with Functional Acyl Homoserine Lactone Lactonase Protein from Bacillus licheniformis and Their Antibiofilm Activity against Proteus Species, Antimicrob Agents Chemother. 59 (2014) 763–771, https://doi.org/10.1128/AAC.03047-14.

[15] L. Yu, F. Shang, X. Chen, J. Ni, L. Yu, M. Zhang, The anti-biofilm effect of silver-nanoparticle-decorated quercetin nanoparticles on a multi-drug resistant Escherichia coli strain isolated from a dairy cow with mastitis, PeerJ 6 (2018) e5711, https://doi.org/10.7717/peerj.5711.

[16] M. Ramasamy, J. Lee, L. Jintae, Development of gold nanoparticles coated with silica containing the antibiofilm drug cinnamaldehyde and their effects on pathogenic bacteria, Int. J. Nanomed. 12 (2017) 2813–2828, https://doi.org/10.2147/IJN.S132784.

[17] T. Monowar, S. Rahman, S.J. Bhore, G. Raju, Silver Nanoparticles Synthesized by Using the Endophytic Bacterium Pantoea ananatis are Promising Antimicrobial Agents against Multidrug Resistant Bacteria, Molecules. 23 (2018) 1–17, https://doi.org/10.3390/molecules23123220.

[18] A. Panáček, L. Kvítek, M. Smékalová, R. Večeřová, M. Kolář, M. Röderová, F. Dyčka, M. Šebela, R. Prucek, O. Tomanec, R. Zbořil, Bacterial resistance to silver nanoparticles and how to overcome it, Nat. Nanotechnol. 13 (2018) 65–71, https://doi.org/10.1038/s41565-017-0013-y.

[19] M.B. Marulasiddeshwara, S.S. Dakshayani, M.N. Sharath Kumar, R. Chethana, P. Raghavendra Kumar, S. Devaraja, Facile-one pot-green synthesis, antibacterial, antifungal, antioxidant and antiplatelet activities of lignin capped silver nanoparticles: A promising therapeutic agent, Mater. Sci. Eng. C. 81 (2017) 182–190, https://doi.org/10.1016/j.msec.2017.07.054.

[20] G. Ferreres, A. Bassegoda, J. Hoyo, J. Torrent-Burgués, T. Tzanov, Metal-Enzyme Nanoaggregates Eradicate Both Gram-Positive and Gram-Negative Bacteria and Their Biofilms, ACS Appl. Mater. Interfaces. 10 (2018) 40434–40442, https://doi.org/10.1021/acsami.8b14949.

[21] A. Ivanova, K. Ivanova, A. Tied, T. Heinze, T. Tzanov, Layer-By-Layer Coating of Aminocellulose and Quorum Quenching Acylase on Silver Nanoparticles Synergistically Eradicate Bacteria and Their Biofilms, Adv. Funct. Mater. 30 (2020) 2001284, https://doi.org/10.1002/adfm.202001284.

[22] L. Mei, Z. Xu, Y. Shi, C. Lin, S. Jiao, L. Zhang, P. Li, Multivalent and synergistic chitosan oligosaccharide-Ag nanocomposites for therapy of bacterial infection, Sci. Rep. 10 (2020) 1–9, https://doi.org/10.1038/s41598-020-67139-7.

[23] B. Rémy, L. Plener, P. Decloquement, N. Armstrong, M. Elias, D. Daudé, É. Chabrière, Lactonase Specificity Is Key to Quorum Quenching in Pseudomonas aeruginosa, Front. Microbiol. 11 (2020) 1–17, https://doi.org/10.3389/fmicb.2020.00762.

[24] R. Sikdar, M. Elias, Evidence for Complex Interplay between Quorum Sensing and Antibiotic Resistance in Pseudomonas aeruginosa, Microbiol. Spectr. 10 (2022), https://doi.org/10.1128/spectrum.01269-22 e01269-22.

[25] P. Nisar, N. Ali, L. Rahman, M. Ali, Z. Khan, M. Ali, Antimicrobial activities of biologically synthesized metal nanoparticles: an insight into the mechanism of action, JBIC J. Biol. Inorg. Chem. 24 (2019) 929–941, https://doi.org/10.1007/s00775-019-01717-7.

[26] L. Wang, C. Hu, L. Shao, The antimicrobial activity of nanoparticles: present situation and prospects for the future, Int J Nanomedicine. 12 (2017) 1227–1249, https://doi.org/10.2147/IJN.S121956.

[27] M. Asif, M. Arif, Green synthesized and characterized copper nanoparticles using various new plants extracts aggravate microbial cell membrane damage after interaction with lipopolysaccharide, Int. J. Biol. Macromol. 160 (2020) 1168–1176, https://doi.org/10.1016/j.ijbiomac.2020.05.198.

[28] I.X. Yin, J. Zhang, I.S. Zhao, M.L. Mei, Q. Li, C.H. Chu, The Antibacterial Mechanism of Silver Nanoparticles and Its Application in Dentistry, Int. J. Nanomed. 15 (2020) 2555–2562, https://doi.org/10.2147/IJN.S246764.

[29] A. Francesko, M. Cano Fossas, P. Petkova, M.M. Fernandes, E. Mendoza, T. Tzanov, Sonochemical synthesis and stabilization of concentrated antimicrobial silver-chitosan nanoparticle dispersions, J. Appl. Polym. Sci. 134 (2017) 1–8, https://doi.org/10.1002/app.45136.

[30] J.T. Davies, E.K. Rideal, Chapter 5—Properties of Monolayers. Interfacial Phenom, 2nd ed., Academic Press, New York, USA, 1961.

[31] S.R. Kadam, H.M.W. den Besten, S. van der Veen, M.H. Zwietering, R. Moezelaar, T. Abee, Diversity assessment of Listeria monocytogenes biofilm formation: Impact of growth condition, serotype and strain origin, Int. J. Food Microbiol. 165 (2013) 259–264, https://doi.org/10.1016/j.ijfoodmicro.2013.05.025.

[32] M.M. Fernandes, K. Ivanova, A. Francesko, D. Rivera, J. Torrent-burgués, A. Gedanken, E. Mendonza, T. Tzanov, Escherichia coli and Pseudomonas aeruginosa eradication by nano-penicillin G, Nanomedicine Nanotechnology, Biol. Med. 12 (2016) 2061–2069, https://doi.org/10.1016/j.nano.2016.05.018.

[33] X. Liu, D. Li, X. Sun, Z. Li, H. Song, H. Jiang, Tunable Dipole Surface Plasmon Resonances of Silver Nanoparticles by Cladding Dielectric Layers, Sci. Rep. 6 (2015) 1–7, https://doi.org/10.1038/srep12555.

[34] L.-H. Li, J.-C. Deng, H.-R. Deng, Z.-L. Liu, X.-L. Li, Preparation, characterization and antimicrobial activities of chitosan/Ag/ZnO blend films, Chem. Eng. J. 160 (2010) 378–382, https://doi.org/10.1016/j.cej.2010.03.051.

[35] O.A. Yeshchenko, I.M. Dmitruk, A.A. Alexeenko, A.V. Kotko, J. Verdal, A. O. Pinchuk, Size and Temperature Effects on the Surface Plasmon Resonance in Silver Nanoparticles, Plasmonics. 7 (2012) 685–694, https://doi.org/10.1007/s11468-012-9359-z.

[36] A.M. Abdelgawad, S.M. Hudson, O.J. Rojas, Antimicrobial wound dressing nanofiber mats from multicomponent (chitosan/silver-NPs/polyvinyl alcohol) systems, Carbohydr. Polym. 100 (2014) 166–178, https://doi.org/10.1016/j.carbpol.2012.12.043.

[37] M.A. Polinarski, A.L.B. Beal, F.E.B. Silva, J. Bernardi-Wenzel, G.R.M. Burin, G.I. B. de Muniz, H.J. Alves, New Perspectives of Using Chitosan, Silver, and Chitosan-Silver Nanoparticles against Multidrug-Resistant Bacteria, Part. Part. Syst. Charact. 38 (2021) 1–18, https://doi.org/10.1002/ppsc.202100009.

[38] A.P. Carapeto, A.M. Ferraria, A.M.B. do Rego, Unraveling the reaction mechanism of silver ions reduction by chitosan from so far neglected spectroscopic features, Carbohydr. Polym. 174 (2017) 601–609. https://doi.org/10.1016/j.carbpol.2017.06.100.

[39] W.Y. Su, Y.C. Chen, F.H. Lin, Injectable oxidized hyaluronic acid/adipic acid dihydrazide hydrogel for nucleus pulposus regeneration, Acta Biomater. 6 (2010) 3044–3055, https://doi.org/10.1016/j.actbio.2010.02.037.

[40] A.A. Hebeish, M.H. El-Rafie, F.A. Abdel-Mohdy, E.S. Abdel-Halim, H.E. Emam, Carboxymethyl cellulose for green synthesis and stabilization of silver nanoparticles, Carbohydr. Polym. 82 (2010) 933–941, https://doi.org/10.1016/j.carbpol.2010.06.020.

[41] D.V. Goia, Preparation and formation mechanisms of uniform metallic particles in homogeneous solutions, J. Mater. Chem. 14 (2004) 451–458, https://doi.org/10.1039/b311076a.

[42] K. Ivanova, A. Ivanova, E. Ramon, J. Hoyo, S. Sanchez-Gomez, T. Tzanov, Antibody-Enabled Antimicrobial Nanocapsules for Selective Elimination of Staphylococcus aureus, ACS Appl. Mater. Interfaces. 12 (2020) 35918–35927, https://doi.org/10.1021/acsami.0c09364.

[43] N.O. Metreveli, K.K. Jariashvili, L.O. Namicheishvili, D.V. Svintradze, E. N. Chikvaidze, A. Sionkowska, J. Skopinska, UV-vis and FT-IR spectra of ultraviolet irradiated collagen in the presence of antioxidant ascorbic acid, Ecotoxicol. Environ. Saf. 73 (2010) 448–455, https://doi.org/10.1016/j.ecoenv.2009.12.005.

[44] M. Filice, M. Marciello, M. del P. Morales, J.M. Palomo, Synthesis of heterogeneous enzyme–metal nanoparticle biohybrids in aqueous media and their applications in C–C bond formation and tandem catalysis, Chem. Commun. 49 (2013) 6876–6878. https://doi.org/10.1039/c3cc42475h.

[45] K. Tanimoto, N. Higashi, M. Nishioka, K. Ishikawa, M. Taya, Characterization of thermostable aminoacylase from hyperthermophilic archaeon Pyrococcus horikoshii, FEBS J. 275 (2008) 1140–1149, https://doi.org/10.1111/j.1742-4658.2008.06274.x.

[46] S. Prabhu, E.K. Poulose, Silver nanoparticles: mechanism of antimicrobial action, synthesis, medical applications, and toxicity effects, Int. Nano Lett. 2 (2012) 32–41, https://doi.org/10.1186/2228-5326-2-32.
[47] J. Li, S. Zhuang, Antibacterial activity of chitosan and its derivatives and their interaction mechanism with bacteria: Current state and perspectives, Eur. Polym. J. 138 (2020) 109984, https://doi.org/10.1016/j.eurpolymj.2020.109984.
[48] P. Gupta, S. Chhibber, K. Harjai, Efficacy of purified lactonase and ciprofloxacin in preventing systemic spread of Pseudomonas aeruginosa in murine burn wound model, Burns. 41 (2015) 153–162, https://doi.org/10.1016/j.burns.2014.06.009.
[49] W. Wang, J. Liu, Y. Huo, J. Ling, Bacteriocin immunity proteins play a role in quorum-sensing system regulated antimicrobial sensitivity of Streptococcus mutans UA159, Arch. Oral Biol. 58 (2012) 384–390, https://doi.org/10.1016/j.archoralbio.2012.09.001.
[50] S. Sethupathy, K. Ganesh, S. Ananthi, S. Mahalingam, Proteomic analysis reveals modulation of iron homeostasis and oxidative stress response in Pseudomonas aeruginosa PAO1 by curcumin inhibiting quorum sensing regulated virulence factors and biofilm production, J. Proteomics. 145 (2016) 112–126, https://doi.org/10.1016/j.jprot.2016.04.019.
[51] S. Morein, A. Andersson, L. Rilfors, Wild-type Escherichia coli Cells Regulate the Membrane Lipid Composition in a window between Gel and Non-lamellar Structures, J. Biol. Chem. 271 (1996) 6801–6809, https://doi.org/10.1074/jbc.271.12.6801.
[52] Y. Tashiro, A. Inagaki, M. Shimizu, S. Ichikawa, N. Takaya, T. Nakajima-Kambe, H. Uchiyama, N. Nomura, Characterization of phospholipids in membrane vesicles derived from Pseudomonas aeruginosa, Biosci. Biotechnol. Biochem. 75 (2011) 605–607, https://doi.org/10.1271/bbb.100754.
[53] J. Hoyo, J. Torrent-Burgués, T. Tzanov, Physical states and thermodynamic properties of model gram-negative bacterial inner membranes, Chem. Phys. Lipids. 218 (2019) 57–64, https://doi.org/10.1016/j.chemphyslip.2018.12.003.
[54] M.M. Fernandes, A. Francesko, J. Torrent-Burgués, T. Tzanov, Effect of thiol-functionalisation on chitosan antibacterial activity: Interaction with a bacterial membrane model, React. Funct. Polym. 73 (2013) 1384–1390, https://doi.org/10.1016/j.reactfunctpolym.2013.01.004.
[55] G. Ferreres, S. Pérez-Rafael, J. Torrent-Burgués, T. Tzanov, Hyaluronic Acid Derivative Molecular Weight-Dependent Synthesis and Antimicrobial Effect of Hybrid Silver Nanoparticles, Int. J. Mol. Sci. 22 (2021) 13428, https://doi.org/10.3390/ijms222413428.
[56] B. Krajewska, P. Wydro, A. Jańczyk, Probing the modes of antibacterial activity of chitosan. Effects of pH and molecular weight on chitosan interactions with membrane lipids in Langmuir films, Biomacromolecules. 12 (2011) 4144–4152, https://doi.org/10.1021/bm2012295.
[57] M.M. Fernandes, A. Francesko, J. Torrent-Burgués, F.J. Carrio, T. Heinze, T. Tzanov, Sonochemically Processed Cationic Nanocapsules: Efficient Antimicrobials with Membrane Disturbing Capacity, Biomacromolecules. 15 (2014) 1365–1374, https://doi.org/10.1021/bm4018947.
[58] Q. Li, S. Mao, H. Wang, X. Ye, The Molecular Architecture of Pseudomonas aeruginosa Quorum-Sensing Inhibitors, Mar. Drugs. 20 (2022) 488, https://doi.org/10.3390/md20080488.
[59] P.D. Utari, R. Setroikromo, B.N. Melgert, W.J. Quax, PvdQ Quorum Quenching Acylase Attenuates Pseudomonas aeruginosa Virulence in a Mouse Model of Pulmonary Infection, Front. Cell. Infect. Microbiol. 8 (2018) 119, https://doi.org/10.3389/fcimb.2018.00119.
[60] W. Dong, J. Zhu, X. Guo, D. Kong, Q. Zhang, Y. Zhou, Characterization of AiiK, an AHL lactonase, from Kurthia huakui LAM0618 T and its application in quorum quenching on Pseudomonas aeruginosa PAO1, Sci. Rep. 8 (2018) 1–11, https://doi.org/10.1038/s41598-018-24507-8.
[61] Z. Xu, Y. Liang, S. Lin, D. Chen, B. Li, L. Li, Y. Deng, Crystal Violet and XTT Assays on Staphylococcus aureus Biofilm Quantification, Curr. Microbiol. 73 (2016) 474–482, https://doi.org/10.1007/s00284-016-1081-1.
[62] R. Sood, D.S. Chopra, Regulatory Approval of Silver Nanoparticles, Appl. Clin. Res. Clin. Trials Regul. Aff. 5 (2018) 74–79, https://doi.org/10.2174/2213476X05666180614121601.
[63] Y. Huang, C. Wu, R.S. Aronstam, Toxicity of Transition Metal Oxide Nanoparticles: Recent Insights from in vitro Studies, Materials (Basel). 10 (2010) 4842–4859, https://doi.org/10.3390/ma3104842.
[64] S.N. Rampersad, Multiple applications of alamar blue as an indicator of metabolic function and cellular health in cell viability bioassays, Sensors. 12 (2012) 12347–12360, https://doi.org/10.3390/s120912347.
[65] J. Hoyo, K. Ivanova, J. Torrent-Burgués, T. Tzanov, Interaction of Silver-Lignin Nanoparticles With Mammalian Mimetic, Membranes 8 (2020) 1–8, https://doi.org/10.3389/fbioe.2020.00439.
[66] K.L.S. Worthington, A.A. Dodd, A. Wongrakpanich, I.A. Mudunkotuwa, K. A. Mapuskar, V.B. Joshi, A. Guymon, D.R. Spitz, V.H. Grassian, P.S. Thorne, A. K. Salem, Chitosan coating of copper nanoparticles reduces in vitro toxicity and increases inflamation in the lung, Nanotechnology. 24 (2013) 1–7, https://doi.org/10.1038/jid.2014.371.